CHIN. PHYS. LETT. Vol. 35, No. 11 (2018) 114301

A Sound Field Separation and Reconstruction Technique Based on Reciprocity Theorem and Fourier Transform *

Xiao-Lei Li(李小雷)[1**], Ning Wang(王宁)[1], Da-Zhi Gao(高大治)[1], Qi Li(李琪)[2]
[1]*Department of Marine Technology, Ocean University of China, Qingdao 266100*
[2]*College of Underwater Acoustic Engineering, Harbin Engineering University, Harbin 150006*

(Received 18 June 2018)

We show a method to separate the sound field radiated by a signal source from the sound field radiated by noise sources and to reconstruct the sound field radiated by the signal source. The proposed method is based on reciprocity theorem and the Fourier transform. Both the sound field and its gradient on a measurement surface are needed in the method. Evanescent waves are considered in the method, which ensures a high resolution reconstruction in the near field region of the signal source when evanescent waves can be measured. A simulation is given to verify the method and the influence of measurement noise on the method is discussed.

PACS: 43.60.+d, 43.60.Sx, 43.60.Jn, 43.60.Lq DOI: 10.1088/0256-307X/35/11/114301

In a noisy environment, sound field separation technique is usually utilized to remove the influence of noise sources for near-field acoustic holography (NAH) applications and various methods about sound field separation have been proposed.[1–9] Weinreich and Arnold proposed a technique for separating outgoing waves from the source and incoming waves from reflections by making the measurement on two closely spaced parallel surfaces.[1] Frisk *et al.* derived a field separation technique based on the spatial Fourier transform (SFT) method for measuring the reflection coefficient in the field of underwater acoustics.[2] Although the SFT method was further developed by several researchers,[3–5] the method requires that the measurement surface must be regular such as planar, cylindrical or spherical. Both the boundary element method (BEM)[6] and the equivalent source method (ESM)[7–9] can be used to cope with the above problem. In the BEM, both pressure and velocity are measured in an enclosed surface, and the standard Helmholtz integral formulation is used to remove the influence of noise sources on the measurement surface. To reconstruct the field in the whole space in the BEM, a sound field reconstruction method is needed. Replacing the radiating body by a system of estimable simple sources located within the envelope of the radiator, ESM can separate the sound field from the sound field radiated by noise sources when pressures in two layers or pressure and velocity in a layer are measured. However, it is difficult and it needs experience to find the optimal positions of the equivalent sources.[10] In this Letter, a method called the reciprocity theorem Fourier transform method (RFTM) is proposed, which combines reciprocity theorem[11,12] and Fourier transform to realize sound field separation and reconstruction. Like BEM and ESM, the RFTM does not need that the measurement surface must be regular. When sound pressure and velocity (or pressure's gradient) are measured on an enclosed measurement surface, sound field separation and reconstruction can be carried out immediately by the RFTM without needing experience, which is different from ESM. Like NAH,[13,14] evanescent waves are considered in the RFTM, which can reconstruct the sound field radiated by a signal source with high accuracy even in the near field of the signal source. The scattering effects of the signal source are neglected in this study, and researchers are referred to the works of Christophe *et al.*[6] and Chuan *et al.*[8] for the relevant analysis.

In this study, the sound field (field means pressure field in the following) is considered in frequency domain which can transform to time domain by

$$f(t) = \int_{-\infty}^{\infty} F(\omega)\exp(-i\omega t)d\omega,$$

where t presents time, ω is the angular frequency, and $i^2 = -1$. Let $\varphi(\boldsymbol{r})$ be the total field radiated by a collection of sound sources $\{S_0, S_1, \ldots, S_N\}$, in which S_0 is the signal source and $S_1, \ldots, S_N$ are noise sources, see Fig. 1(a). Then $\varphi(\boldsymbol{r})$ satisfies the inhomogeneous Helmholtz equation

$$\nabla^2\varphi(\boldsymbol{r}) + k^2\varphi(\boldsymbol{r}) = \sum_{n=0}^{N} S_n(\boldsymbol{r}), \tag{1}$$

where $k = \omega/c$ is wave number and c is sound speed in the medium. Suppose source S_0 is in a domain D whose boundary is ∂D, while the other sources are not included in the domain D, as shown in Fig. 1(a). Then the total field in the domain D satisfies

$$\nabla^2\varphi(\boldsymbol{r}) + k^2\varphi(\boldsymbol{r}) = S_0(\boldsymbol{r}), \quad \boldsymbol{r} \in D. \tag{2}$$

The sound field radiated by $S_0(\boldsymbol{r})$ is presented by $\varphi_0(\boldsymbol{r})$, then $\varphi_0(\boldsymbol{r})$ satisfies

$$\nabla^2\varphi_0(\boldsymbol{r}) + k^2\varphi_0(\boldsymbol{r}) = S_0(\boldsymbol{r}), \tag{3}$$

which is the same as Eq. (2) except that $\boldsymbol{r}$ is not limited in D. It is well known that $\varphi_0(\boldsymbol{r})$ can be expressed

*Supported by the National Natural Science Foundation of China under Grant Nos 11374270 and 11674294.
**Corresponding author. Email: LXL_ouc@163.com

as

$$\varphi_0(\boldsymbol{r}) = \int_D S_0(\boldsymbol{r}_0) G(\boldsymbol{r}, \boldsymbol{r}_0) d\boldsymbol{r}_0, \tag{4}$$

where $G(\boldsymbol{r}, \boldsymbol{r}_0)$ is Green's function in free space and satisfies

$$\nabla^2 G(\boldsymbol{r}, \boldsymbol{r}_0) + k^2 G(\boldsymbol{r}, \boldsymbol{r}_0) = \delta(\boldsymbol{r} - \boldsymbol{r}_0). \tag{5}$$

Expanding $G(\boldsymbol{r}, \boldsymbol{r}_0)$ by plan waves[15,16]

$$G(\boldsymbol{r}, \boldsymbol{r}_0) = \int_\Omega \alpha(\boldsymbol{k}_r) \exp[i\boldsymbol{k}_r \cdot (\boldsymbol{r}^h - \boldsymbol{r}_0^h) \pm ik_z(z - z_0)] d\boldsymbol{k}_r, \tag{6}$$

where $\mathrm{Im}(k_z) \geqslant 0$, $\boldsymbol{k} = (\boldsymbol{k}_r, k_z)$, $\boldsymbol{r} = (\boldsymbol{r}^h, z)$, $+$ is used when $z \geqslant z_0$, $-$ is used when $z < z_0$, $\|\boldsymbol{k}\|_2 = k$ and the other parameters are listed in Table 1. Substitute Eq. (6) into Eq. (4) and we consider only the situation $z \geqslant z_0$ in the following.

Table 1. Some parameters in Eq. (6) in two- and three-dimensional cases.

	$\boldsymbol{r}^h$	$\boldsymbol{k}_r$	$\alpha(\boldsymbol{k}_r)$	Ω
Two-dimension	x	k_x	$-i/(4\pi k_z)$	$\{k_x \mid -\infty < k_x < \infty\}$
Three-dimension	(x, y)	(k_x, k_y)	$-i/(8\pi^2 k_z)$	$\{k_r \mid (k_x^2 + k_y^2) < \infty\}$

Similar analysis can be used in $z < z_0$. One obtains

$$\varphi_0(\boldsymbol{r}) = \int_\Omega \alpha(\boldsymbol{k}_r) \exp(i\boldsymbol{k}_r \cdot \boldsymbol{r}^h + ik_z z) \int_D S_0(\boldsymbol{r}_0) \exp(-i\boldsymbol{k}_r \cdot \boldsymbol{r}_0^h - ik_z z_0) d\boldsymbol{r}_0 d\boldsymbol{k}_r. \tag{7}$$

According to the reciprocity theorem,[11,12] the integral with respect to $\boldsymbol{r}_0$ in Eq. (7) can be computed by the total field $\varphi(\boldsymbol{r})$ and its gradient $\nabla\varphi(\boldsymbol{r})$ on the measurement surface ∂D,

$$\begin{aligned}\beta(\boldsymbol{k}_r) &= \int_D S_0(\boldsymbol{r}_0) \exp(-i\boldsymbol{k}_r \cdot \boldsymbol{r}_0^h - ik_z z_0) d\boldsymbol{r}_0 \\ &= \oint_{\partial D} [\exp(-i\boldsymbol{k} \cdot \boldsymbol{r}_0) \nabla_{\boldsymbol{r}_0} \varphi(\boldsymbol{r}_0) \\ &\quad - \varphi(\boldsymbol{r}_0) \nabla_{\boldsymbol{r}_0} \exp(-i\boldsymbol{k} \cdot \boldsymbol{r}_0)] \cdot \boldsymbol{n} dS,\end{aligned} \tag{8}$$

where $\nabla_{\boldsymbol{r}_0}$ is the gradient operator with respect to $\boldsymbol{r}_0$ and $\boldsymbol{n}$ is the unit normal vector in outward direction of ∂D, and the detail derivation can be found in Ref. [11]. From Eq. (8), it is found that both the pressure $\varphi(\boldsymbol{r})$ and the normal velocity $v_n(\boldsymbol{r}) \propto \nabla\varphi(\boldsymbol{r}) \cdot \boldsymbol{n}$ on the boundary ∂D should be measured to obtain $\beta(\boldsymbol{k}_r)$. Combining Eqs. (7) and (8), one obtains

$$\varphi_0(\boldsymbol{r}) = \int_\Omega \alpha(\boldsymbol{k}_r) \beta(\boldsymbol{k}_r) \exp(i\boldsymbol{k}_r \cdot \boldsymbol{r}^h + ik_z z) d\boldsymbol{k}_r. \tag{9}$$

Now, we obtain the field $\varphi_0(\boldsymbol{r})$ according to the total field $\varphi(\boldsymbol{r})$, and Eq. (9) is the final form of the RFTM. From Eqs. (8) and (9) one can find that the shape of measurement surface can be arbitrary as long as the last integral in Eq. (8) exists and the sound field radiated by $S_0(\boldsymbol{r})$ is just the Fourier transform of $\alpha(\boldsymbol{k}_r)\beta(\boldsymbol{k}_r)\exp(ik_z z)$.

To verify the validation of the RFTM, a simulation in the two-dimensional case is given.

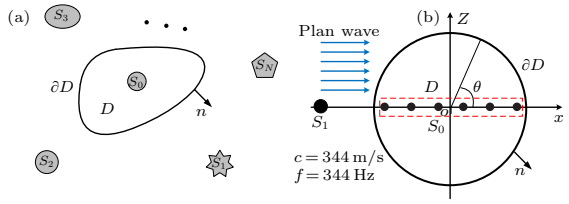

Fig. 1. Schematic diagram of the RFTM. (a) Geometry of the RFTM based sound field separation technique. Only source S_0 is in the domain D. Measurement surface is ∂D and $\boldsymbol{n}$ is the unit vector in the normal direction of ∂D. (b) Sketch map of the simulation environment. Here S_0 is composed of six identity point sources with unit strength and the origin of coordinate system located at its center. The distance between neighbor point sources of S_0 is 0.4 m, and S_1 is a point source at $(-2\,\mathrm{m}, 0)$, and its strength equals 10. A plane wave with unit amplitude propagates along the x direction. Domain D is a circle area whose radius is 1.1 m and centered at the origin of coordinated system, and 360 measurement points distribute uniformly on ∂D which is the boundary of D.

A sketch map of the simulation environment is given in Fig. 1(b). The frequency of sound f is 344 Hz, sound speed c is 344 m/s in the space, and the corresponding wavelength λ is 1 m. The signal source S_0 is composed of six identity point sources with unit strength and origin of coordinate system located at its center, as shown in Fig. 1(b). The distance between neighbor point sources of S_0 is 0.4 m, which is less than half of the wavelength. The noise source S_1 is a point source at $(-2\,\mathrm{m}, 0)$, and its strength equals 10. A plane wave with unit amplitude propagates along the x direction. Then the total field can be expressed as

$$\varphi(\boldsymbol{r}) = \underbrace{\int \sum_{n=1}^{6} \delta(\boldsymbol{r}' - \boldsymbol{r}_n^0) G_0(\boldsymbol{r}, \boldsymbol{r}') d\boldsymbol{r}'}_{\varphi_0(\boldsymbol{r})} + \underbrace{10 \int \delta(\boldsymbol{r}' - \boldsymbol{r}^1) G_0(\boldsymbol{r}, \boldsymbol{r}') d\boldsymbol{r}' + \exp(ikx)}_{\text{Interference}},$$

where $\boldsymbol{r} = (x, z)$ are the spatial coordinates, $\boldsymbol{r}_n^0$ are the spatial coordinates of the nth point source in S_0,

$\boldsymbol{r}^1$ are the spatial coordinates of S_1, $k = 2\pi/\lambda$ is the wavenumber, and

$$G_0(\boldsymbol{r}, \boldsymbol{r}') = -\frac{i}{4} H_0^{(1)}(k|\boldsymbol{r} - \boldsymbol{r}'|)$$

is Green's function in two-dimensional free space. Domain D is a circle area whose radius R is 1.1 m and centered at the origin of the coordinate system in the space. Here 360 measurement points distribute uniformly on ∂D which is the boundary of D. Note that D is just an area of human choice in the space and ∂D is not a physical boundary. The total field $\varphi(\boldsymbol{r})$ and its gradient $\nabla\varphi(\boldsymbol{r})$ are measured by the measurement points. Substitute $\varphi(\boldsymbol{r})$ and $\nabla\varphi(\boldsymbol{r})$ into Eqs. (8) and (9), $\varphi_0(\boldsymbol{r})$ which is the field radiated by S_0 can be reconstructed. When using the last integral of Eq. (8) to compute $\beta(\boldsymbol{k}_r)$, $\nabla_{\boldsymbol{r}_0}\varphi(\boldsymbol{r}_0)\cdot\boldsymbol{n}$ is approximated by the finite difference method. Note that the integral region of Eq. (9) in the two-dimensional case is $\{k_x|-\infty < k_x < \infty\}$, which is not feasible in numerical calculation. In this simulation, the integral region of Eq. (9) is changed to $\{k_x| - \xi k < k_x < \xi k\}$ with a finite real number ξ, and the sound field radiated by S_0 is approximated by

$$\tilde{\varphi}_0(\boldsymbol{r}, \xi) = \int_{-\xi k}^{\xi k} \alpha(k_x)\beta(k_x)\exp(ik_x x + ik_z z)dk_x. \quad (10)$$

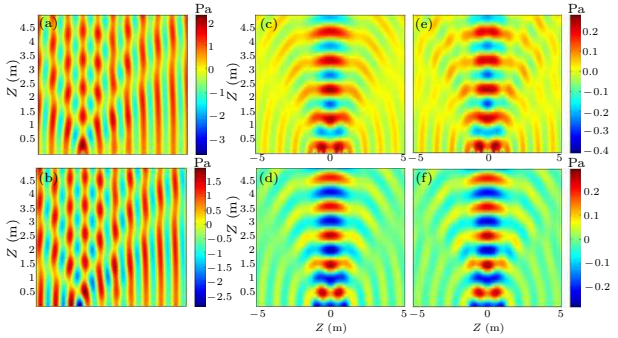

Fig. 2. Spatial distribution of the sound field. (a) Real part of the total field $\varphi(\boldsymbol{r})$. (b) Image part of the total field $\varphi(\boldsymbol{r})$. (c) Real part of $\varphi_0(\boldsymbol{r})$ which is the field radiated by S_0. (d) Image part of $\varphi_0(\boldsymbol{r})$. (e) Real part of the field $\tilde{\varphi}_0(\boldsymbol{r}, \xi = 4)$ which is the separated field by the RFTM. (f) Image part of the field $\tilde{\varphi}_0(\boldsymbol{r}, \xi = 4)$.

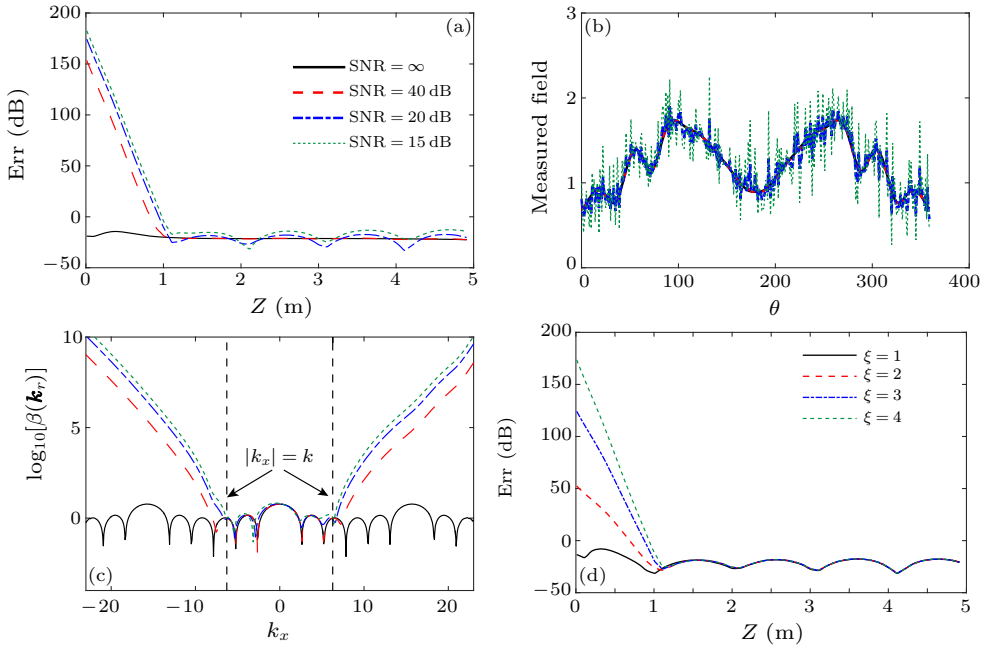

Fig. 3. The effect of noise on the RFTM. (a) Relative error between $\tilde{\varphi}_0(\boldsymbol{r}, \xi)$ and $\varphi_0(\boldsymbol{r})$ under different SNR conditions when $\xi = 4$ and $\boldsymbol{r} = \{(x, z)|x = 0, 0 < z \leqslant 5\}$. (b) Measured field $\varphi^N(\boldsymbol{r})$ under different SNRs. (c) The value of $\log_{10}\beta(\boldsymbol{k}_r)$ under different SNR conditions. (d) Relative error between $\tilde{\varphi}_0(\boldsymbol{r}, \xi)$ and $\varphi_0(\boldsymbol{r})$ when SNR=20 dB and $\boldsymbol{r} = \{(x, z)|x = 0, 0 < z \leqslant 5\}$ under different ξ.

The simulation results are shown in Fig. 2. The real part and the imaginary part of the total field $\varphi(\boldsymbol{r})$ are given in Figs. 2(a) and 2(b), respectively, which are very different from the field radiated by S_0 as shown in Figs. 2(c) and 2(d). The real part and imaginary part of $\tilde{\varphi}_0(\boldsymbol{r}, \xi)$ obtained by Eq. (10) are given in Figs. 2(e) and 2(f), respectively. One can find that $\tilde{\varphi}_0(\boldsymbol{r}, \xi)$ is nearly the same as $\varphi_0(\boldsymbol{r})$ even in the near field of S_0. In addition, the locations of different point sources of S_0 can be identified as shown in Fig. 2(e), even though the distance between neighbor point sources of S_0 is less than half the wavelength for the evanescent waves considered in the RFTM. Defining relative error between $\tilde{\varphi}_0(\boldsymbol{r}, \xi)$ and $\varphi_0(\boldsymbol{r})$ as

$$Err(\boldsymbol{r}, \xi) = 20\log_{10}\frac{|\tilde{\varphi}_0(\boldsymbol{r}, \xi) - \varphi_0(\boldsymbol{r})|}{|\varphi_0(\boldsymbol{r})|}, \quad (11)$$

and Fig. 3(a) gives the relative error when $\xi = 4$ and $\boldsymbol{r} = \{(x, z)|x = 0, 0 < z \leqslant 5\}$. In practice, both $\varphi(\boldsymbol{r})$ and its gradient will be contaminated by measurement noise during the measurement process. Then the mea-

sured total field and its derivative in the normal direction on ∂D are

$$\varphi^N(\boldsymbol{r}) = \varphi(\boldsymbol{r}) + n_1(\boldsymbol{r}), \tag{12}$$

$$\nabla\varphi^N(\boldsymbol{r}) \cdot \boldsymbol{n} = \nabla\varphi(\boldsymbol{r}) \cdot \boldsymbol{n} + n_2(\boldsymbol{r}), \tag{13}$$

where $n_1(\boldsymbol{r})$ and $n_2(\boldsymbol{r})$ are noise terms and satisfy $\langle n_1(\boldsymbol{r}_i)n_1^*(\boldsymbol{r}_j)\rangle = \sigma^2\delta_{ij}$, $\langle n_2(\boldsymbol{r}_i)n_2^*(\boldsymbol{r}_j)\rangle = k^2\sigma^2\delta_{ij}$, $\langle n_1(\boldsymbol{r}_i)n_2^*(\boldsymbol{r}_j)\rangle = 0$, $\langle\rangle$ refers to average, $\boldsymbol{r}_i$ and $\boldsymbol{r}_j$ are two points in the space, $*$ refers to complex conjugation, and δ_{ij} is the Kronecker delta function. For the convenience of analysis, the signal-to-noise ratio (SNR) is defined as

$$\mathrm{SNR} = 10\log_{10}\Big[\frac{1}{N\sigma^2}\sum_{n=1}^{N}|\varphi(\boldsymbol{r}_n)|^2\Big], \tag{14}$$

where N is the total number of the measurement points on ∂D, and $\boldsymbol{r}_n$ is the location of the nth measurement point. Assuming that both $n_1(\boldsymbol{r})$ and $n_2(\boldsymbol{r})$ satisfy complex Gauss distribution with zero mean, Fig. 3(b) gives the measured total field $\varphi^N(\boldsymbol{r})$ varies with θ (θ is defined in Fig. 1(b)) under different SNRs. The relative errors between $\tilde{\varphi}_0(\boldsymbol{r},\xi)$ and $\varphi_0(\boldsymbol{r})$ under different SNR conditions are shown in Fig. 3(a) when $\xi = 4$. From Fig. 3(a), it is suggested that the measurement noise has significant influence on $\tilde{\varphi}_0(\boldsymbol{r},\xi)$ when $z < 1$ m. From Eq. (8), one can find that the measurement noise influences $\beta(\boldsymbol{k}_r)$ exponentially when $|k_x| > k$, see Fig. 3(c), which has significant influence on $\tilde{\varphi}_0(\boldsymbol{r},\xi)$ in $z < R$. It can also be found from Fig. 3(d) that when $|k_x| > k$ or $\xi > 1$, the greater the allowed $|k_x|$ or ξ is, the stronger the influence of the measurement noise on $\tilde{\varphi}_0(\boldsymbol{r},\xi)$ in $z < R$.

In summary, a sound field separation and reconstruction technique called the reciprocity theorem Fourier transform method has been proposed. Both pressure field and its gradient need be measured on an enclosed measurement surface in the method. A simulation is given to verify the validity of the RFTM. Measurement noise's influence on the RFTM is discussed and it shows that the measurement noise will have a strong influence on the near field of the signal source S_0 when evanescent waves are considered. In the real application of the RFTM, both the total field $\varphi(\boldsymbol{r})$ and its gradient $\nabla\varphi(\boldsymbol{r})$ need to be measured on a measurement surface ∂D, then sound field separation and reconstruction can be realized by Eqs. (8) and (9). How many measurement points on the measurement surface are needed in the RFTM is not discussed in this study. When using numerical methods to calculate the last integral in Eq. (8), the accuracy of the integral calculation depends on the number of measurement points on the measurement surface. If researchers intend to further knowledge about the relation between the number of measurement points and the accuracy of the integral calculation, please refer to any numerical analysis books for the relevant analysis.

We thank Gaokun Yu for useful discussion, and Jing Chi, Xinyao Zhang and Shuangshuang Jiang for useful suggestions about writing.

References

[1] Weinreich G and Arnold E B 1980 *J. Acoust. Soc. Am.* **68** 404
[2] Frisk G V, Oppenheim A V and Martinez D R 1980 *J. Acoust. Soc. Am.* **68** 602
[3] Yu F, Chen J, Li W B et al 2005 *Acta Phys. Sin.* **54** 789 (in Chinese)
[4] Tamura M, Allard J F and Lafarge D 1995 *J. Acoust. Soc. Am.* **97** 2255
[5] Cheng M T, Mann J A and Pate A 1995 *J. Acoust. Soc. Am.* **97** 2293
[6] Langrenne C, Melon M and Garcia A 2007 *J. Acoust. Soc. Am.* **121** 2750
[7] Bi C X, Hu D Y, Zhang Y B et al 2013 *Acta Phys. Sin.* **62** (in Chinese) 084301
[8] Bi C X, Hu D Y, Zhang Y B et al 2013 *J. Acoust. Soc. Am.* **134** 2823
[9] Bi C X, Jing W Q, Zhang Y B et al 2017 *J. Sound Vib.* **386** 149
[10] Ochmann M 1995 *Acta Acust. United Acust.* **81** 512
[11] Li X L, Yu G K, Wang N et al 2017 *J. Acoust. Soc. Am.* **141** EL1
[12] Lin J, Li X L and Wang N 2016 *Chin. Phys.* B **25** 124303
[13] Williams E G and Maynard J D 1980 *Phys. Rev. Lett.* **45** 554
[14] Maynard J D, Williams E G and Lee Y 1985 *J. Acoust. Soc. Am.* **78** 1395
[15] Sheng P 2006 *Introduction to Wave Scattering, Localization and Mesoscopic Phenomena* (New York: Springer)
[16] Brekhovskikh L M, Lysanov Y P and Beyer R T 1991 *Fundamentals of Ocean Acoustics* (New York: Springer)